

Curve Veering of Eigenvalue Loci of Bridges with Aeroelastic Effects

Xinzhong Chen¹ and Ahsan Kareem²

Abstract: The eigenvalues of bridges with aeroelastic effects are commonly portrayed in terms of a family of frequency and damping loci as a function of mean wind velocity. Depending on the structural dynamic and aerodynamic characteristics of the bridge, when two frequencies approach one another over a range of wind velocities, their loci tend to repel, thus avoiding an intersection, whereas the mode shapes associated with these two frequencies are exchanged in a rapid but continuous way as if the curves had intersected. This behavior is referred to as the curve veering phenomenon. In this paper, the curve veering of cable-stayed and suspension bridge frequency loci is studied. A perturbation series solution is utilized to estimate the variations of the complex eigenvalues due to small changes in the system parameters and establish the condition under which frequency loci veer, quantified in terms of the difference between adjacent eigenvalues and the level of mode interaction. Prior to the discussion of bridge frequency loci, the curve veering of a two-degree-of-freedom system comprised of a primary structure and tuned mass damper is discussed, which not only provides new insight into the dynamics of this system, but also helps in understanding the veering of bridge frequency loci. To study this more complicated dynamic system, a closed-form solution of a two-degree-of-freedom coupled flutter is obtained, and the underlying physics associated with the heaving branch flutter is discussed in light of the veering of frequency loci. It is demonstrated that the concept of curve veering in bridge frequency loci provides a correct explanation of multimode coupled flutter analysis results for long span bridges and helps to improve understanding of the underlying physics of their aeroelastic behavior.

DOI: 10.1061/(ASCE)0733-9399(2003)129:2(146)

CE Database keywords: Eigenvalues; Bridges, span; Aeroelasticity.

Introduction

Wind-bridge interaction results in the generation of self-excited forces, which provide additional aerodynamic damping and stiffness to that already present in the structure. In addition, these self-excited forces induce aerodynamic coupling of structural modes, changing the eigenmodes of the bridge. Therefore, the real-valued structural modes are only observed when the mean wind velocity is zero, while complex modes are present under wind excitation. To avoid confusion, these complex modes are referred to as complex mode branches. The eigenvalues associated with complex mode branches can be estimated utilizing a complex eigenvalue analysis (e.g., Katsuchi et al. 1999; Chen et al. 2000). These eigenvalues are commonly portrayed in terms of a family of frequency and damping loci as a function of mean wind velocity.

The behavior of these loci has interesting ramifications for the bridge flutter problem. Depending on the structural dynamic and

aerodynamic characteristics of the bridge, two adjacent frequency loci may approach each other over a range of wind velocities. When this occurs, the curves may intersect or repel each other. However, even in the case where the curves repel each other, the eigenmodes (eigenvectors) associated with these two eigenvalues are exchanged continuously as if the curves had intersected (Chen et al. 2001). This behavior has been termed the “curve veering phenomenon.”

Because of this ambiguous behavior of frequency loci, traditional flutter analysis that employs an iterative calculation procedure, based on frequency-dependent state-space equation, has proven to be computationally cumbersome. In this approach, the target mode identification has to be done iteratively, which may not permit complete automation of the analysis procedure (Chen et al. 2000).

This behavior of frequency loci may also result in coupled multimode flutter, involving more than two structural modes, which may initiate from a complex mode branch that is different from the commonly observed torsional mode branch. For example, in multimode bridge flutter analyses, it has been shown that a suspension bridge coupled flutter initiated from a lateral mode branch (Miyata and Yamada 1988; Chen et al. 2000; Chen et al. 2001), and a cable-stayed bridge coupled flutter initiated from a mode branch associated with a tower bending mode as the wind velocity increased (Chen et al. 2001). This behavior may give the impression that the physics of the multimode coupled flutter is different from the general understanding of coupled flutter in which two fundamental structural modes of the bridge deck, i.e., heaving and torsional fundamental structural modes, are most important. This general understanding of coupled flutter has been the foundation of both the analytical bimodal flutter predictions and wind tunnel based spring-supported section model studies.

¹Postdoctoral Research Associate, Dept. of Civil Engineering and Geological Sciences, Univ. of Notre Dame, Notre Dame, IN 46556. E-mail: xchen@nd.edu

²Professor and Chair, Dept. of Civil Engineering and Geological Sciences, Univ. of Notre Dame, Notre Dame, IN 46556. E-mail: kareem@nd.edu

Note. Associate Editor: Roger G. Ghanem. Discussion open until July 1, 2003. Separate discussions must be submitted for individual papers. To extend the closing date by one month, a written request must be filed with the ASCE Managing Editor. The manuscript for this paper was submitted for review and possible publication on February 28, 2002; approved on May 20, 2002. This paper is part of the *Journal of Engineering Mechanics*, Vol. 129, No. 2, February 1, 2003. ©ASCE, ISSN 0733-9399/2003/2-146-159/\$18.00.

However, as a result of the contributions to aerodynamic damping arising from aerodynamic coupling among structural modes, it has been demonstrated that the multimode flutter is physically consistent with bimodal flutter, although consideration of higher modes offers a more accurate prediction (Chen et al. 2000; Chen et al. 2001). In addition, the coupled self-excited force components acting on the bridge deck, i.e., lift due to torsional motion and pitching moment due to heaving motion, play a critical role in developing negative aerodynamic damping. While the understanding of the multimode flutter has been significantly improved, the behavior of adjacent bridge frequency loci and the conditions under which they repel rather than intersect have yet to be clearly understood.

Recent studies of coupled flutter using spring-supported bridge section models have shown that even in the case of bimodal flutter, the heaving branch may also be the origin of so-called "heaving branch coupled flutter" (Matsumoto et al. 1999). The physics of this type of flutter has not yet been fully identified. This type of flutter may be related to the behavior of adjacent bridge frequency loci as discussed previously for the multimode coupled flutter.

This veering phenomenon has also manifested itself in a wide range of other fields, following its initial identification in the study of crystals by Anderson (1958), who coined the term "curve veering." Later, Leissa (1974) demonstrated veering of eigenvalue loci due to the approximate vibration mode analysis of a rectangular membrane. Nair and Durvasula (1973) showed analytically that the natural frequencies of plates belonging to the same symmetry group yield the veering phenomena when plotted versus geometric parameters, such as the skew angle and side ratio, proposing a criterion for identifying the conditions under which the eigenvalue loci veer rather than cross. Perkins and Mote (1986) studied the conditions under which the eigenvalue loci veer for a general real-valued eigenvalue problem utilizing a perturbation method, while Pierre (1988) discussed the relationship between veering of the eigenvalue loci and mode localization. This work was continued by Chen and Ginsberg (1992) who established criteria governing the occurrence of veering and studied the relationship between the veering of eigenvalue loci and the parameter sensitivity of eigenvectors, in which the perturbation series solution utilized included the adjacent eigenvectors at the zeroth-order expansion (Nair and Durvasula 1973). The curve veering phenomenon for eigenvalues of a system dependent on one or two parameters has also been discussed by Morand and Ohayon (1995).

In this paper, a perturbation series solution is presented to estimate the variations of the complex eigenvalues due to small changes in the system parameters. Based on the perturbation series solution, the curve veering of cable-stayed and suspension bridge frequency loci is studied to establish the condition under which frequency loci veer. In order to better understand this phenomenon, the curve veering of a structure with a tuned mass damper (TMD) is first discussed using a two-degree-of-freedom (2DOF) model. After illustrating the curve veering phenomenon in the familiar structure-TMD system, this concept is used to explore the underlying physics associated with heaving branch flutter in the 2DOF coupled flutter of bridges. The discussion of curve veering offers new insights into the dynamics of the structure-TMD system, provides a correct explanation of the results of the multimode coupled flutter analysis, and helps to improve understanding of the underlying physics of long span bridge aeroelastic behavior.

Perturbation Analysis of Eigenvalue Problem

The eigenvalue problem of a dynamic system with a system matrix \mathbf{A} is expressed as

$$\mathbf{A}\Phi_j = \lambda_j\Phi_j \quad (1)$$

where λ_j and Φ_j = j th eigenvalue and eigenvector (eigenmode).

It is insightful to consider the variations of eigenvalues and eigenvectors due to small changes in the system matrix \mathbf{A} to $\mathbf{A} + \epsilon\mathbf{A}_0$, where $\epsilon\mathbf{A}_0$ = variation of the system matrix, and ϵ = small perturbation parameter. The system described by matrix \mathbf{A} is referred to as the unperturbed system, and the j th eigenvalue λ_j and eigenvector Φ_j of the perturbed system with a system matrix $\mathbf{A} + \epsilon\mathbf{A}_0$ is given by

$$(\mathbf{A} + \epsilon\mathbf{A}_0)\Phi'_j = \lambda'_j\Phi'_j \quad (2)$$

Assuming that $\lambda_i, \dots, \lambda_k$ are a set of adjacent eigenvalues of the unperturbed system, the corresponding eigenvalue and eigenvector matrices are expressed as

$$\mathbf{\Lambda} = \text{diag}[\lambda_i, \dots, \lambda_k]; \quad \mathbf{\Gamma} = [\Phi_i, \dots, \Phi_k] \quad (3)$$

The perturbed eigenvector Φ'_j ($i \leq j \leq k$) can be expressed in terms of the eigenvectors of the unperturbed system, in which the adjacent eigenvectors are included in the zeroth-order expansion

$$\Phi'_j = \mathbf{\Gamma}\mathbf{D} + \epsilon\mathbf{\Gamma}_1\mathbf{E} \quad (4)$$

where $\mathbf{\Gamma}_1$ = the eigenvector matrix of the unperturbed system excluding $\mathbf{\Gamma}$; and \mathbf{D} and \mathbf{E} = the coefficient vectors.

Substituting Eq. (4) into Eq. (2) and multiplying by the left-hand side eigenvector matrix of \mathbf{A} corresponding to $\mathbf{\Lambda}$, i.e., $\mathbf{\Gamma}_L$, leads to a system equation for λ'_j and \mathbf{D}

$$(\mathbf{\Lambda} + \epsilon\mathbf{H})\mathbf{D} = \lambda'_j\mathbf{D} \quad (5)$$

where \mathbf{H} is defined as

$$\mathbf{H} = \mathbf{\Gamma}_L\mathbf{A}_0\mathbf{\Gamma} \quad (6)$$

and $\mathbf{\Gamma}_L$ satisfies the following:

$$\mathbf{\Gamma}_L\mathbf{A} = \mathbf{\Gamma}_L\mathbf{\Lambda}; \quad \mathbf{\Gamma}_L\mathbf{\Gamma} = \mathbf{I}; \quad \mathbf{\Gamma}_L\mathbf{A}\mathbf{\Gamma}_1 = \mathbf{0} \quad (7)$$

Accordingly, the λ'_j and \mathbf{D} can be determined through the solution of the eigenvalue problem defined in Eq. (5), which provides a relationship among the modal properties of the unperturbed and perturbed systems.

In the following, the case where only two eigenvalues of the unperturbed system are adjacent is considered, and the corresponding eigenvalues and eigenvectors of the perturbed system are discussed. For the sake of illustration, these adjacent eigenvalues are written as λ_1 and λ_2 , accordingly reducing Eq. (5) to

$$\begin{bmatrix} \lambda_1 + \epsilon H_{11} & \epsilon H_{12} \\ \epsilon H_{21} & \lambda_2 + \epsilon H_{22} \end{bmatrix} \begin{bmatrix} D_{1j} \\ D_{2j} \end{bmatrix} = \lambda'_j \begin{bmatrix} D_{1j} \\ D_{2j} \end{bmatrix} \quad (8)$$

The solution of the preceding equation leads to the eigenvalues λ'_j ($j = 1, 2$):

$$\lambda'_j = \frac{1}{2}(\lambda_1^* + \lambda_2^*) \mp \frac{1}{2}[(\lambda_1^* - \lambda_2^*)^2 + 4\epsilon^2 H_{12}H_{21}]^{1/2} \quad (9)$$

with the eigenvectors (normalized to unit):

$$\begin{aligned} D_{1j} &= -\epsilon H_{12} / \sqrt{(\lambda_1^* - \lambda_j')^2 + \epsilon^2 H_{12}^2} \\ D_{2j} &= (\lambda_1^* - \lambda_j') / \sqrt{(\lambda_1^* - \lambda_j')^2 + \epsilon^2 H_{12}^2} \end{aligned} \quad (10)$$

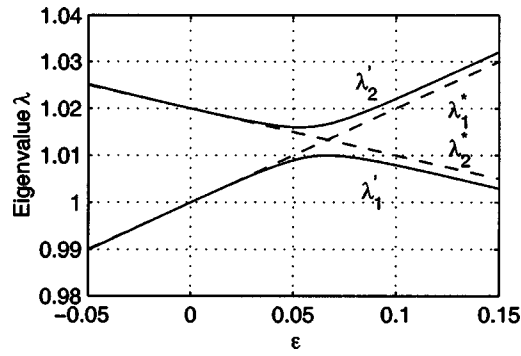


Fig. 1. General picture of curve veering of eigenvalue loci

where λ_j^* ($j=1,2$)=the eigenvalues of the unperturbed system corrected for the influence of the diagonal terms of matrix $\epsilon\mathbf{H}$

$$\lambda_1^* = \lambda_1 + \epsilon H_{11}; \quad \lambda_2^* = \lambda_2 + \epsilon H_{22} \quad (11)$$

It is obvious that $H_{12}=H_{21}=0$ leads to $\lambda_j' = \lambda_j^*$ and $\Phi_j' = \Phi_j$, indicating that the existence of the diagonal terms of $\epsilon\mathbf{H}$ only modifies the eigenvalues but does not influence the eigenmodes of the unperturbed system.

The eigenvectors of the perturbed system in the zeroth-order expansion are then given by

$$\Phi_j' = D_{1j}\Phi_1 + D_{2j}\Phi_2 \quad (12)$$

In the case where $\epsilon\mathbf{A}$ and \mathbf{A}_0 are real-valued symmetric matrices, $\epsilon\mathbf{H}$ becomes a real-valued symmetric matrix, and the eigenvalues and eigenvectors of both unperturbed and perturbed systems are real valued. However, note that in the case of bridges with aeroelastic effects, the system matrix including aerodynamic stiffness and damping terms are nonsymmetric (see the Appendix), thus the eigenvalues and eigenvectors of both the unperturbed and perturbed systems are generally complex valued and the matrix $\epsilon\mathbf{H}$ is generally nonsymmetric.

Detailed discussion on the curve veering of real-valued eigenvalue loci can be found in Chen and Ginsberg (1992) and Morand and Ohayon (1995) based on Eq. (9). A general picture of curve veering of eigenvalue loci is plotted in Fig. 1, and the corresponding eigenmodes are shown in Table 1. The following parameters were used in this numerical example: $\lambda_1 = 1.0$, $\lambda_2 = 1.02$, $H_{11} = 0.2$, $H_{22} = -0.1$, and $H_{12} = H_{21} = 0.05$. It is evident that λ_1^* and λ_2^* intersect at $\epsilon = 0.0667$. However, λ_1' and λ_2' are generally different, where λ_1' and λ_2' denote lower and upper eigenvalues of the perturbed system, respectively. The presence of the off-diagonal terms of $\epsilon\mathbf{H}$ results in separation of the eigenvalues. As pointed out by Chen and Ginsberg (1992) and Morand and Ohayon (1995) and as indicated by Fig. 1 and Table 1, during the

Table 1. Eigenmodes of Example

ϵ	Mode 1		Mode 2	
	D_{11}	D_{21}	D_{12}	D_{22}
0.02	-1.00	0.07	0.07	1.00
0.04	-0.97	0.23	0.23	0.97
0.06	-0.81	0.58	0.58	0.81
0.0667	-0.71	0.71	0.71	0.71
0.08	-0.53	0.85	0.85	0.53
0.10	-0.38	0.92	0.92	0.38
0.12	-0.32	0.95	0.95	0.32

veering, the eigenvector associated with λ_1' changes from $-\Phi_1$ to Φ_2 , passing through $(-\Phi_1 + \Phi_2)/\sqrt{2}$. In the same way, the eigenvector associated with λ_2' changes from Φ_2 to Φ_1 , passing through $(\Phi_1 + \Phi_2)/\sqrt{2}$.

For a general complex eigenvalue problem, the curve veering of frequency loci can be explained as follows. From Eq. (9), it is obvious that only when

$$\Delta = [(\lambda_1^* - \lambda_2^*)^2 + 4\epsilon^2 H_{12}H_{21}]^{1/2} = 0 \quad (13)$$

two adjacent eigenvalues are equal, i.e.,

$$\lambda_1' = \lambda_2' = \frac{1}{2}(\lambda_1^* + \lambda_2^*) \quad (14)$$

This means that both the frequency and damping ratio loci of the two adjacent complex modes intersect. Since, in general, Δ is not necessarily equal to zero, the frequencies or damping ratios of the two adjacent complex modes will generally be different from each other.

As shown in Eqs. (9) and (10) and Fig. 1 and Table 1, at the region where λ_1^* and λ_2^* are sufficiently distinct, i.e., $|\lambda_1^* - \lambda_2^*| \gg 2\epsilon|(H_{12}H_{21})^{1/2}|$, the interaction between adjacent modes is weak, and the eigenvalues and eigenvectors of the perturbed system, λ_j' and Φ_j' , are close to λ_j^* and Φ_j .

On the other hand, at the region where λ_1^* and λ_2^* are sufficiently adjacent, i.e., $|\lambda_1^* - \lambda_2^*| \approx 2\epsilon|(H_{12}H_{21})^{1/2}|$, the mode interaction between adjacent modes is strong, and the eigenvalues are significantly influenced by the term $2\epsilon(H_{12}H_{21})^{1/2}$. The curve veering exists, and the eigenvectors Φ_1' and Φ_2' result from a significant coupling between Φ_1 and Φ_2 . During curve veering, the eigenvectors (eigenmodes) of the perturbed system are apparently different from those for which λ_1^* and λ_2^* are sufficiently distinct, and the eigenmodes exhibit dramatic yet continuous change with variations of the perturbation parameters. This phenomenon is referred to as mode shape localization.

The following criterion can be utilized to identify the existence of curve veering, i.e., when

$$d = |\lambda_1^* - \lambda_2^*| / [2\epsilon|(H_{12}H_{21})^{1/2}|] \leq O(1) \quad (15)$$

the frequency loci veer, otherwise, these intersect. It is noted that the mode interaction index, d , represents the distance between two eigenvalues of the unperturbed system which have been corrected to include the influence of the diagonal terms of perturbation matrix $\epsilon\mathbf{H}$, normalized by the off-diagonal terms of $\epsilon\mathbf{H}$. A lower value of the mode interaction index corresponds to a stronger modal interaction.

Expressing the complex eigenvalues, λ_j^* ($j=1,2$), in terms of their frequencies, ω_j^* , and damping ratios, ξ_j^*

$$\lambda_j^* = -\xi_j^* \omega_j^* + i \omega_j^* \sqrt{1 - (\xi_j^*)^2} \quad (16)$$

the difference in the eigenvalues of the adjacent complex modes can be approximated as follows when the frequencies are close to each other

$$|\lambda_1^* - \lambda_2^*| \approx \omega^* |\xi_1^* - \xi_2^*| \quad (17)$$

where $\omega_1^* \approx \omega_2^* \approx \omega^*$. Consequently, the curve veering of frequency loci is obviously related to the difference in the damping ratios of these two adjacent modes compared to $2\epsilon(H_{12}H_{21})^{1/2}$.

Curve Veering of Frequency Loci of Structure-Tuned Mass Damper System

Although the thrust of this work is focused on the veering of bridge frequency loci, a 2DOF structure-TMD system is chosen

as a simple, first example to illustrate the veering phenomenon of frequency loci. The free vibration of the structure–TMD system can be described in the following nondimensional state-space equations

$$\begin{Bmatrix} y_s' \\ y_t' \\ y_s'' \\ y_t'' \end{Bmatrix} = \begin{bmatrix} 0 & 0 & 1 & 0 \\ 0 & 0 & 0 & 1 \\ -(1 + \mu_m \mu_f^2) & \mu_m \mu_f^2 & -2\xi_s - 2\mu_m \xi_t \mu_f & 2\mu_m \xi_t \mu_f \\ \mu_f^2 & -\mu_f^2 & 2\xi_t \mu_f & -2\xi_t \mu_f \end{bmatrix} \begin{Bmatrix} y_s \\ y_t \\ y_s' \\ y_t' \end{Bmatrix} \quad (18)$$

where $\mu_m = m_t/m_s$ = the mass ratio; $\mu_f = \omega_t/\omega_s$ = the tuning frequency ratio; m , ξ , and ω = the mass, damping ratio, and frequency, respectively; y = the displacement; subscripts s and t = the structure and TMD, respectively; and the prime denotes the derivative with respect to the nondimensional time $\tau = \omega_s t$. It is obvious that the dynamics of the structure–TMD system depends on the mass ratio μ_m , tuning frequency ratio μ_f , TMD damping ratio ξ_t , and structural damping ratio ξ_s . The effect of structural damping, which is generally small, can be neglected.

The eigenvalues of the structure–TMD system can be calculated through the complex eigenvalue analysis based on the preceding state-space equations. These can also be estimated based on a perturbation analysis. The system consisting of the isolated structure and TMD is chosen as the unperturbed system with state-space equations

$$\begin{Bmatrix} y_s' \\ y_t' \\ y_s'' \\ y_t'' \end{Bmatrix} = \begin{bmatrix} 0 & 0 & 1 & 0 \\ 0 & 0 & 0 & 1 \\ -1 & 0 & -2\xi_s & 0 \\ 0 & -\mu_f^2 & 0 & -2\xi_t \mu_f \end{bmatrix} \begin{Bmatrix} y_s \\ y_t \\ y_s' \\ y_t' \end{Bmatrix} \quad (19)$$

with eigenvalues

$$\lambda_1 = -\xi_s + i\sqrt{1 - \xi_s^2}; \quad \lambda_2 = -\xi_t \mu_f + i\mu_f \sqrt{1 - \xi_t^2} \quad (20)$$

and eigenvectors

$$\Phi_1 = [1 \ 0 \ \lambda_1 \ 0]^T; \quad \Phi_2 = [0 \ 1 \ 0 \ \lambda_2]^T \quad (21)$$

By expressing the eigenvectors of the structure–TMD system in terms of those of the unperturbed system, the eigenvalue and eigenvectors of the perturbed system can be estimated based on Eqs. (9) and (10) with the matrix $\epsilon \mathbf{H}$ given by

$$\epsilon \mathbf{H} = -0.5i \begin{bmatrix} -\mu_m \mu_f (\mu_f + 2\xi_t \lambda_1) / \sqrt{1 - \xi_s^2} & \mu_m \mu_f (\mu_f + 2\xi_t \lambda_2) / \sqrt{1 - \xi_s^2} \\ (\mu_f + 2\xi_t \lambda_1) / \sqrt{1 - \xi_t^2} & 0 \end{bmatrix} \quad (22)$$

It is noted that the perturbation series solution results in exactly the same solutions of modal properties as the direct complex eigenvalue analysis [Eq. (18)]. This is due to that fact that the two equations are strictly equivalent and are related by a transformation of the modal coordinates of the isolated structure and TMD.

In Fig. 2, the frequencies, damping ratios and eigenmodes in terms of the amplitude ratios between the TMD and the structure for two complex modes versus frequency ratio μ_f varying from 0.8 to 1.2 with $\xi_t = 5\%$, $\xi_s = 0\%$, and $\mu_m = 1\%$ are presented. Fig. 3 shows the results for the same parameters as Fig. 2 with the exception of $\xi_t = 12\%$. The modal interaction index for these two cases are calculated based on Eq. (15) and are presented in Figs. 2(d) and 3(d).

The cure veering of frequency loci for the case of $\xi_t = 5\%$ is observed. The upper frequency locus (dashed line) corresponds to the structure dominated mode in the range of a lower-frequency ratio which changes to the TMD dominated mode at a higher-frequency ratio locale. On the other hand, the lower-frequency locus (solid line) changes from the TMD dominated mode to the structure dominated mode as the frequency ratio increased. The cure veering is due to a strong interaction between the TMD and the structure as indicated by Fig. 2(d). In the case of $\xi_t = 12\%$, higher TMD damping resulted in a relatively weak interaction between the TMD and the structure [Fig. 3(d)] such that the frequency loci intersect like those of the isolated TMD and the structure system (unperturbed system).

The modal properties of the structure–TMD system suggest that there are generally two distinct frequencies for a given set of parameters except when $\mu_f = (\mu_f)_{\text{opt}} = 1/(1 + \mu_m)$ and $\xi_t \geq (\xi_t)_{\text{opt}} = \sqrt{\mu_m}$, where $(\mu)_{\text{opt}}$ and $(\xi_t)_{\text{opt}}$ are the optimal frequency tuning ratio and damping ratio of TMD with $\xi_s = 0$. It is clear from Fig. 4, which shows the modal frequencies of the structure–TMD system at $\mu_f = (\mu_f)_{\text{opt}}$, that the two frequencies coalesce only when $\xi_t \geq (\xi_t)_{\text{opt}}$. Obviously, when the frequency loci of structure–TMD system are plotted versus the frequency ratio μ_f , the two loci will veer for $\xi_t < (\xi_t)_{\text{opt}}$ and intersect for $\xi_t \geq (\xi_t)_{\text{opt}}$ at $\mu_f = (\mu_f)_{\text{opt}}$. However, it is emphasized that despite the veering or intersection of the frequency loci, the physics of the structure–TMD interaction are exactly the same.

Curve Veering of Eigenvalue Loci of Bridges with Aeroelastic Effects

Long Span Cable-Stayed Bridge

A wind-excited cable-stayed bridge with a center span of about 1000 m was chosen as an example to illustrate the curve veering of eigenvalue loci in bridges (Chen et al. 2001). The logarithmic decrement for each structural mode was assumed to be 0.02. For the sake of illustrating the fundamental characteristics of bridges with aeroelastic effects, only the aerodynamic forces acting on the bridge deck were included. The self-excited drag component in-

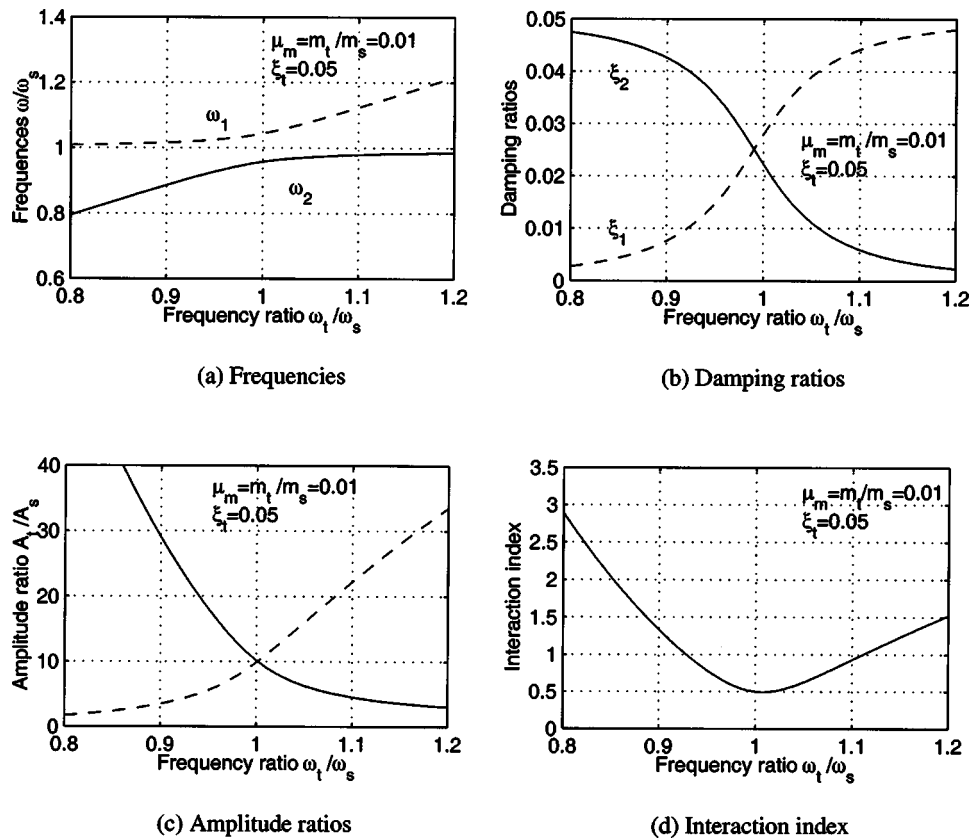


Fig. 2. Modal properties and interaction index of structure-tuned mass damper system ($\xi_t=0.05$)

duced by the lateral motion was calculated based on the quasi-steady theory. The coupled self-excited force components between the lateral and vertical motions and between the lateral and torsional motions are generally negligible and, therefore, were neglected. The flutter derivatives H_i^* and A_i^* ($i=1,2,3,4$) were calculated using the Theodorsen function.

The variations of the bridge frequencies and damping ratios as the wind velocity increases are shown in Fig. 5. These were calculated utilizing the complex eigenvalue analysis of the linear invariant state-space formulations with augmented aerodynamic states (see the Appendix). In the calculation, only several important structural modes, modes 3, 7, 10, and 13, were considered, where modes 3 and 13 are the fundamental vertical bending and torsional modes, respectively; mode 7 is the bending mode of the tower in the bridge plane; and mode 10 is the second symmetric lateral bending mode of the bridge deck. The critical flutter velocity (U_{cr}) was predicted to be 114.1 m/s, which is close to 113.8 m/s based on the first 20 structural modes. The eigenvalue loci of these four complex mode branches are also very close to those based on the first 20 structural modes. The results predicted by only including the two fundamental structural modes (3 and 13) are also plotted for comparison as the dashed lines in Fig. 5 with U_{cr} of 119.3 m/s. The mode shapes of these four complex mode branches are summarized in Table 2 in terms of the amplitude ratios of the structural modal components. The phase lag information is not present herein for the sake of brevity. The structural mode shapes were normalized in accordance with the maximum translateral displacement or torsional displacement of the bridge deck multiplied by the half width of the bridge deck to be unity.

It is noted that at low wind velocities, the complex mode shapes are dominated by their respective real-valued structural

modes, along with coupled components of the other structural modes. At the wind velocities of about 100 m/s, the frequencies of complex mode branches 10 and 13 approach each other without intersecting. Consequently, the mode shapes of these two mode branches exhibit strong coupling. Both modes contain significant contributions from structural modes 10 and 13 with an additional coupled component of structural mode 3 and only a small component of structural mode 7. As wind velocity increases, the mode shapes of complex mode branches 10 and 13 are gradually exchanged to the complex modes dominated by structural modes 13 and 10, respectively. At the wind velocities of about 112 m/s, the frequencies of complex mode branches 7 and 10 are close to each other which results in a significant coupling of these modes. Before this wind velocity range, complex mode 7 is actually structural mode 7, and beyond this range, it becomes a coupled complex mode consisting structural modes 3, 10, and 13. On the other hand, beyond this range, complex mode 10 turned to be dominated by the structural mode 7. The veering of frequency loci between complex mode branches 10 and 13 was noted around the wind velocity of 100 m/s, and between complex mode branches 7 and 10 around the wind velocity of 112 m/s, respectively. The mode shapes associated with these two pairs of eigenvalues are exchanged during veering in a rapid but continuous way as if the curves has intersected. In the curve veering range, mode shape localization is observed, which is attributed to the interaction of these two adjacent complex modes. Taking into account the presence of the veering of frequency loci, the physics of the multi-mode coupled flutter consisting of more than two structural modes is actually the same as the flutter predicted from the analysis based on the two fundamental modes. Both scenarios have dominant contributions of the two fundamental modes to flutter

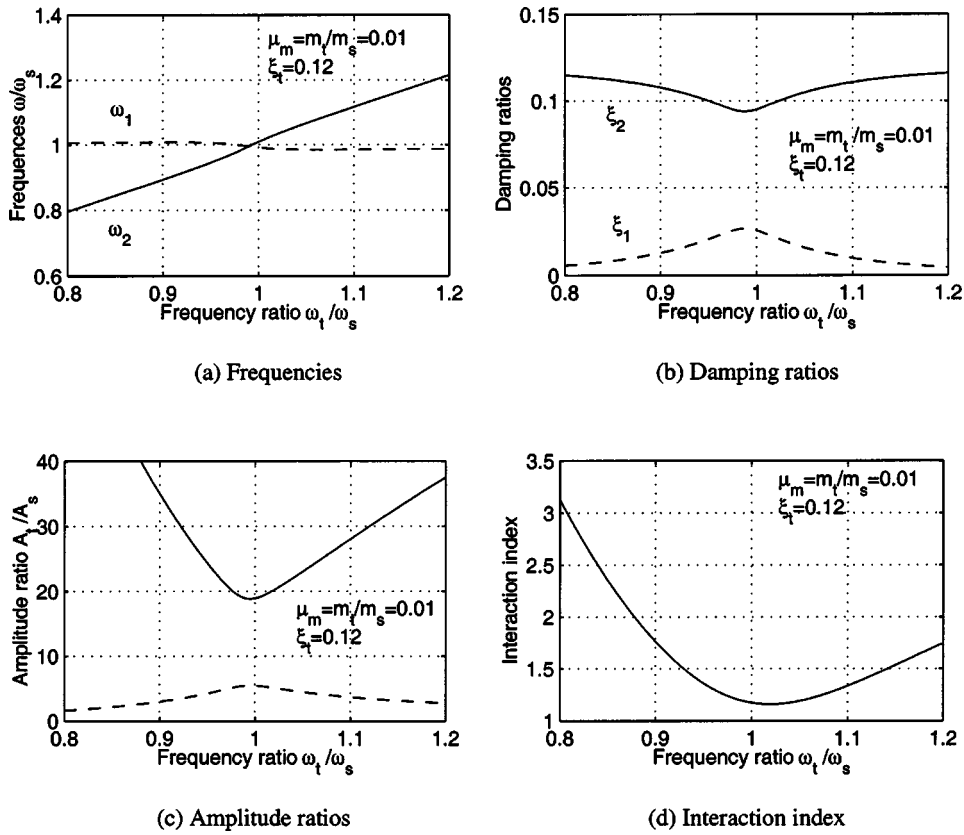


Fig. 3. Modal properties and interaction index of structure–tuned mass damper system ($\xi_t = 0.12$)

and similar variations of frequency and damping loci with increasing wind velocity.

A perturbation analysis was conducted to describe the eigenvalue loci around the two veering regions and, more importantly, to discuss the curve veering conditions. For the discussion of the veering between complex mode branches 10 and 13, the unperturbed system was chosen as the system excluding the coupled aerodynamic terms of structural mode 10 with other structural modes, i.e., modes 3, 7, and 13. This was realized by eliminating the corresponding elements in the aerodynamic matrices \mathbf{A}_s and \mathbf{A}_d (see the Appendix). It is worth noting that the eigenvalues of the unperturbed system corresponding to mode branches 3, 7, and 13 are actually the same as the case considering only structural modes 3, 7, and 13, and that of mode branch 10 is the same as the case considering only the single structural mode 10. The per-

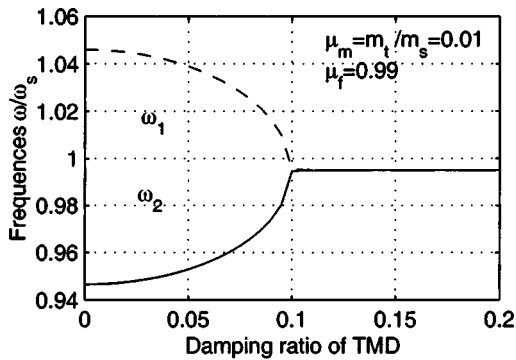
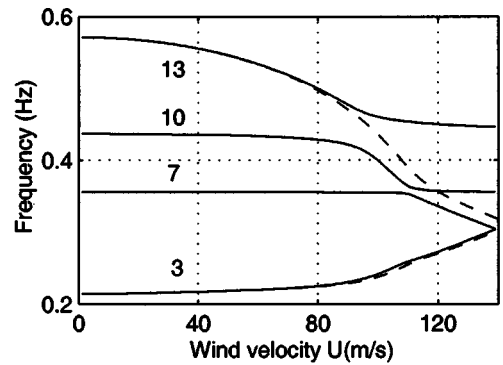
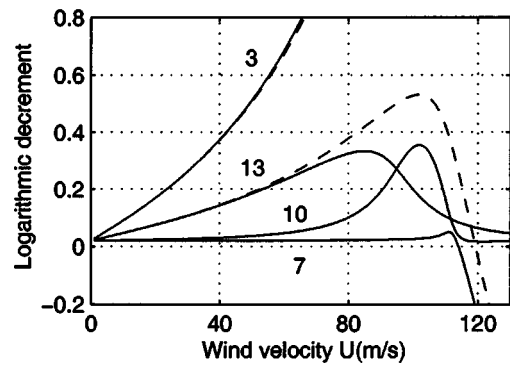


Fig. 4. Frequencies of structure–tuned mass damper system at $\mu_f = (\mu_f)_{opt}$



(a) Frequency vs. wind velocity



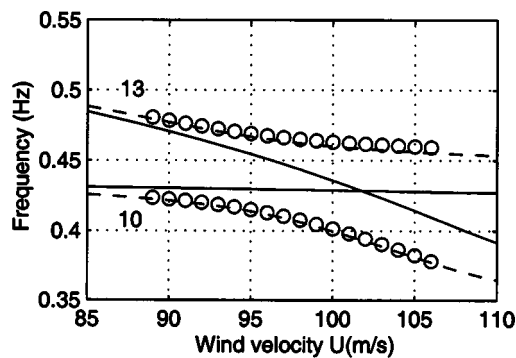
(b) Damping ratio vs. wind velocity

Fig. 5. Eigenvalue loci of cable-stayed bridge (— with structural modes 3,7,10,13; -- with structural modes 3 and 13)

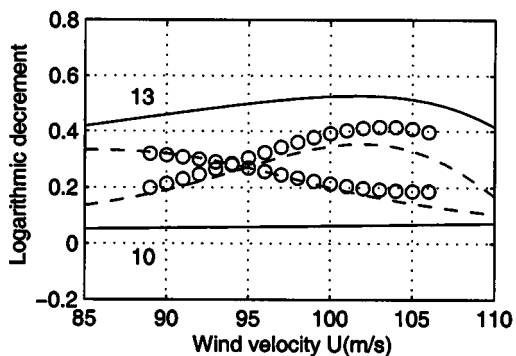
Table 2. Amplitude Ratios of Structural Modes in Complex Mode Branches (the Cable-Stayed Bridge)

U (m/s)	Mode Branch 7				Mode Branch 10				Mode Branch 13			
	3	7	10	13	3	7	10	13	3	7	10	13
90	0.09	1.00	0.03	0.04	0.57	0.04	1.00	0.50	0.55	0.03	0.48	1.00
95	0.13	1.00	0.04	0.05	0.88	0.07	1.00	0.72	0.63	0.03	0.69	1.00
100	0.20	1.00	0.05	0.08	1.43	0.13	1.00	1.00	0.69	0.04	0.95	1.00
105	0.36	1.00	0.09	0.14	2.27	0.27	1.00	1.25	0.73	0.04	1.22	1.00
110	1.00	1.00	0.25	0.38	3.26	0.90	1.00	1.43	0.76	0.04	1.47	1.00
112	1.95	1.00	0.45	0.72	3.51	1.77	1.00	1.47	0.77	0.04	1.47	1.00
114	3.32	1.00	0.70	1.15	3.65	2.97	1.00	1.49	0.77	0.04	1.66	1.00
120	9.44	1.00	1.60	2.80	3.95	8.06	1.00	1.52	0.80	0.04	1.92	1.00
130	21.44	1.00	2.63	5.11	4.23	16.63	1.00	1.55	0.82	0.05	2.31	1.00

turbed system is the original system accounting for all uncoupled terms (diagonal terms) and coupled terms (off-diagonal terms) in \mathbf{A}_s and \mathbf{A}_d at the same wind velocity as the unperturbed system. Therefore, the difference between the unperturbed and perturbed systems is due to the aerodynamic intermode coupling terms of structural mode 10 with other structural modes. Only adjacent mode branches 10 and 13 of the unperturbed system were included in the zero-order expansion.



(a) Frequency vs. wind velocity



(b) Damping ratio vs. wind velocity

Fig. 6. Comparison of eigenvalue loci of complex mode branches 10 and 13 (— and - - - are calculated by complex eigenvalue analysis with and without coupled terms of structural mode 10 with other structural modes; circles are calculated by perturbation analysis): (a) frequency versus wind velocity and (b) damping ratio versus wind velocity

The eigenvalues of the unperturbed system were predicted using the complex eigenvalue analysis (see the Appendix) and are plotted as solid lines in Fig. 6. For this example and the following examples of the perturbation analysis of bridge eigenvalues, the perturbation in the system matrix only results in the existence of the off-diagonal terms of the matrix $\epsilon\mathbf{H}$, thus the eigenvalues λ_i^* are the same as the eigenvalues of the unperturbed system, i.e., $\lambda_i = \lambda_i^*$. It is evident that the frequency loci of mode branches 10 and 13 of the unperturbed system intersect. The eigenvalues of the perturbed system were estimated based on the perturbation series solution [Eq. (9)] (circles in Fig. 6) and were compared to those based on the complex eigenvalue analysis (see the Appendix) (dashed lines). Excellent agreement of the results demonstrated the efficacy of the perturbation series solution. It was also demonstrated that the veering of frequency loci between mode branches 10 and 13 was due to the aerodynamic intermode coupling terms of structural mode 10 with other structural modes. Based on the perturbation analysis, the interaction index of these two complex modes was calculated as shown in Fig. 7. It is obvious that the curve veering corresponds to a low value of this index, representing a strong mode interaction. This demonstrates the utility of the criterion for identifying the onset of curve veering. Similar results for complex modes 7 and 10 at wind velocities around 112 m/s are presented in Figs. 8 and 9. Results again reaffirmed the efficacy of the perturbation series solution and demonstrated that the aerodynamic coupling terms of structural mode 7 with other structural modes resulted in veering of the eigenvalue loci.

In Fig. 6, a slight difference can be observed in the predicted damping ratios of the perturbed system between those based on the perturbation series solution and the direct complex eigenvalue analysis. It was attributed to the contribution of complex mode

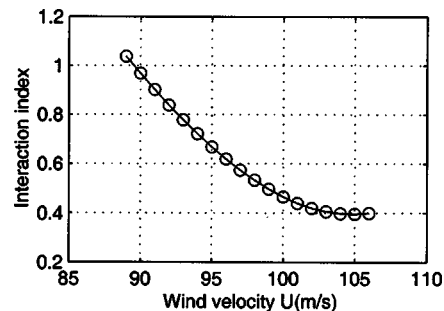
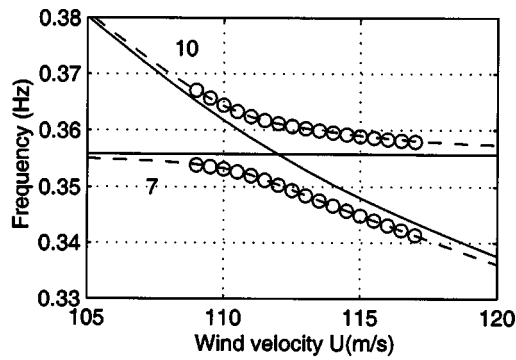
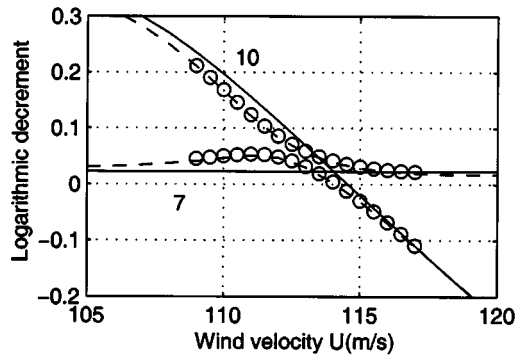


Fig. 7. Interaction index of adjacent complex mode branches 10 and 13



(a) Frequency vs. wind velocity



(b) Damping ratio vs. wind velocity

Fig. 8. Comparison of eigenvalue loci of complex mode branches 7 and 10 (— and — are calculated by complex eigenvalue analysis with and without coupled terms of structural mode 7 and other structural modes; circles are calculated by perturbation analysis): (a) frequency versus wind velocity and (b) damping ratio versus wind velocity

branch 3 of the unperturbed system to the eigenvalues of mode branches 10 and 13 of the perturbed system. This effect can be included by taking into account this complex mode branch along with complex mode branches 10 and 13 in the zeroth-order expansion of the perturbation analysis. Accordingly, a more accurate perturbation series solution can be obtained by including more mode components in the zeroth-order expansion as shown in Fig. 10.

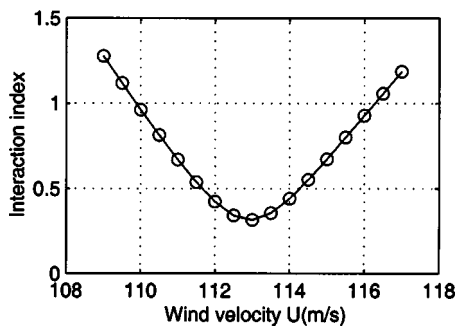


Fig. 9. Interaction index of adjacent complex mode branches 7 and 10

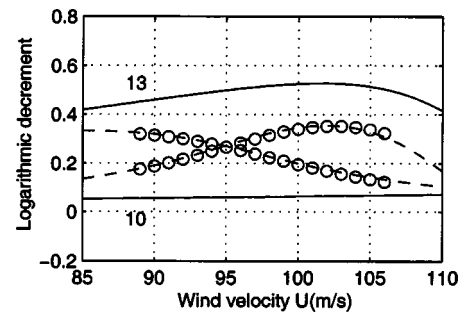
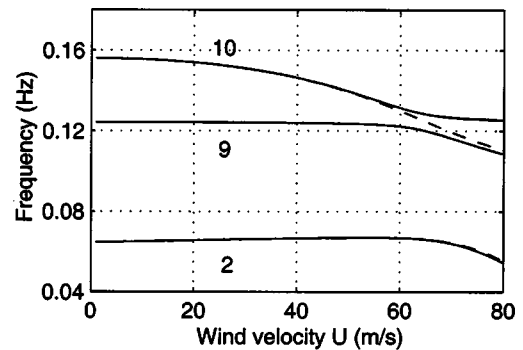


Fig. 10. Comparison of damping loci of complex mode branches 10 and 13 (— and — are calculated by complex eigenvalue analysis with and without coupled terms of structural mode 10 and other structural modes; circles are calculated by perturbation analysis with three adjacent modes)

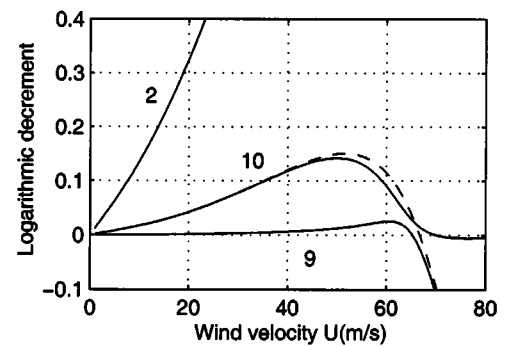
Long-Span Suspension Bridge

A wind-excited long-span suspension bridge with a center span of nearly 2,000 m was used as another example to illustrate the veering of eigenvalue loci (Chen et al. 2000). The logarithmic decrement for each structural mode was assumed to be 0.02. The modeling of the self-excited forces was the same as the aforementioned cable-stayed bridge.

Calculations with different mode combinations using a complex eigenvalue analysis were conducted for estimating the eigenvalues with increasing wind velocity. It was found that the analy-



(a) Frequency vs. wind velocity



(b) Damping ratio vs. wind velocity

Fig. 11. Eigenvalue loci of the suspension bridge (— with structural modes 2,9,10; — with structural modes 2 and 10): (a) frequency versus wind velocity and (b) damping ratio versus wind velocity

Table 3. Amplitude Ratios of Structural Modes in Complex Mode Branches (the Suspension Bridge)

U (m/s)	Mode Branch 9			Mode Branch 10		
	2	9	10	2	9	10
60	0.44	1.00	0.37	0.73	0.53	1.00
62	0.60	1.00	0.49	0.79	0.71	1.00
64	0.84	1.00	0.65	0.85	0.94	1.00
66	1.15	1.00	0.84	0.90	1.22	1.00
68	1.55	1.00	1.05	0.93	1.55	1.00
70	2.04	1.00	1.27	0.96	1.91	1.00
75	3.51	1.00	1.80	1.02	2.84	1.00
80	5.18	1.00	2.22	1.05	3.68	1.00

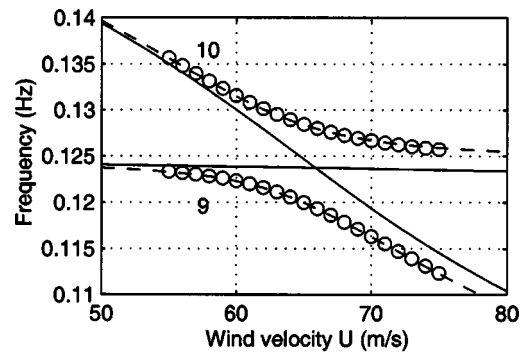
sis including structural modes 2,9,10, which are the fundamental vertical symmetric bending, second lateral symmetric bending, and fundamental torsional symmetric modes, respectively, resulted in U_{cr} of 65.3 m/s, which is close to 66.5 m/s based on the first 15 natural modes. The eigenvalue loci are also similar to a coupled flutter initiated from complex mode branch 9 as indicated by solid lines in Fig. 11. In Table 3, the complex mode shapes of these complex mode branches, in terms of the amplitude ratios of the structural mode components, are presented. The structural mode shapes were normalized in accordance with the maximum translateral displacement or torsional displacement of the bridge deck multiplied by the half width of the bridge deck to be unity.

At around 65 m/s, the eigenvalues of complex mode branches 9 and 10 are close to each other without intersection. The mode shapes of both complex modes consist of strongly coupled components of structural modes 9 and 10 with an additional coupled component of the structural mode 2. As wind velocity exceeds 65 m/s, complex mode 9 gradually transitions to a mode dominated by coupled components of structural modes 2 and 10. In the same way, complex mode 10 gradually changes to the mode dominated by structural mode 9. The veering of frequency loci between complex mode branches 9 and 10 occurs around a wind velocity of 65 m/s. Mode shape localization again occurs in branches 9 and 10 during the veering, indicated by the coupling of structural mode 9 with other structural modes. Away from the veering region, the coupling of structural mode 9 becomes marginal. As compared to the eigenvalues based on the two fundamental modes (structural modes 2 and 10) as shown in dashed lines in Fig. 11, it is clear that the underlying physics of the multimode coupled flutter involving more than two modes is essentially the same as the two mode coupled flutter, despite the fact that the flutter appears to be initiated from different branches.

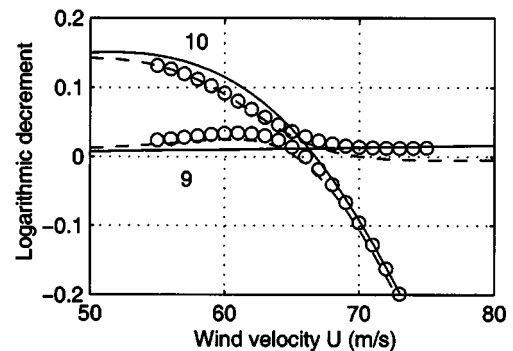
A perturbation analysis was conducted for estimating the eigenvalue loci of complex modes 9 and 10 around the wind velocity of 65 m/s. The perturbation series solution was based on adjacent complex modes 9 and 10 at the same wind velocity predicted by neglecting some of the off-diagonal terms in the aerodynamic matrices \mathbf{A}_s and \mathbf{A}_d representing the coupled terms between structural modes 9 and 2, and between structural modes 9 and 10. It is worth noting that the eigenvalues of the unperturbed system corresponding to mode branches 2 and 10 are actually the same as the case considering only structural modes 2 and 10, and that of mode branch 9 is the same as the case considering only the single structural mode 9. Therefore, the difference between the unperturbed and perturbed systems is due to the aerodynamic intermode coupling terms of structural mode 9 with other modes. Solid and dashed lines in Fig. 12 represent the eigenvalues of the unperturbed and the perturbed systems based on

the complex eigenvalue analysis [Eq. (45)], respectively. Circles represent the results estimated by the perturbation series solution [Eq. (9)]. These results illustrate that the behavior of eigenvalue loci can be accurately described by the perturbation series solution. The corresponding interaction index is shown in Fig. 13, indicating that a strong interaction between complex mode branches 9 and 10 around a wind velocity of 65 m/s resulted in the veering of frequency loci.

For comparison, the flutter analysis considering structural modes 2, 8, and 10 was also conducted, where mode 8 is the second symmetric vertical bending mode. The frequency and damping ratio loci are shown in Fig. 14, in which the dashed and solid lines are the results with and without the off-diagonal terms in aerodynamic matrices \mathbf{A}_s and \mathbf{A}_d representing the aerodynamic coupling between structural modes 8 and 2, and between structural modes 8 and 10. Fig. 15 shows the interaction index of complex modes 8 and 10. The relatively large values of this parameter indicate that the eigenvalue loci are only slightly influenced by the weak interaction of complex mode branches 8 and 10. As a result, the frequency loci of these branches remain intersected. The weak interaction is due to the remarkable difference in the damping ratios of these two mode branches compared to the term $2\epsilon(H_{12}H_{21})^{1/2}$.



(a) Frequency vs. wind velocity



(b) Damping ratio vs. wind velocity

Fig. 12. Comparison of eigenvalue loci of complex mode branches 9 and 10 for the suspension bridge (— and — are calculated by complex eigenvalue analysis with and without coupled terms of structural mode 9 with other structural modes; circles are calculated by perturbation analysis): (a) frequency versus wind velocity and (b) damping ratio versus wind velocity

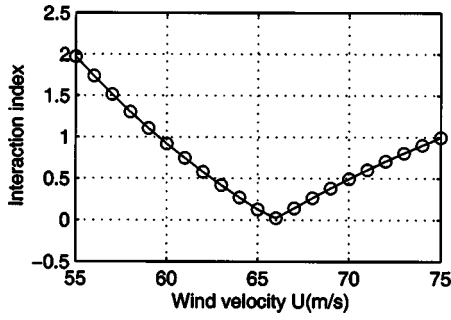


Fig. 13. Interaction index of adjacent complex mode branches 9 and 10 for suspension bridge

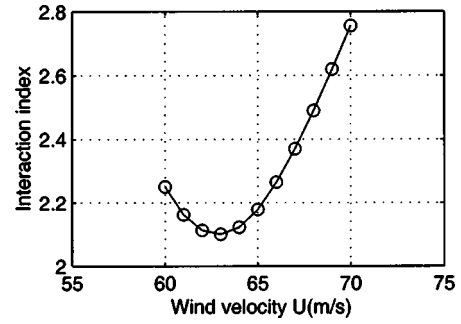


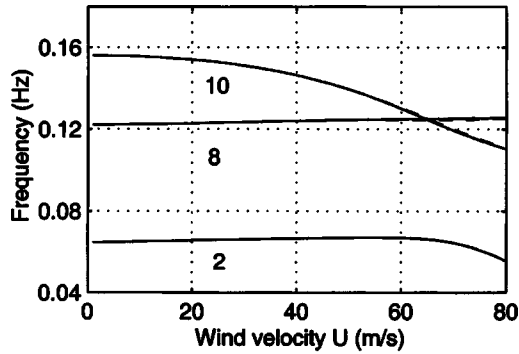
Fig. 15. Interaction index of adjacent complex mode branches 8 and 10 for suspension bridge

Curve Veering of Frequency Loci of Two-Degree-of-Freedom Coupled Flutter

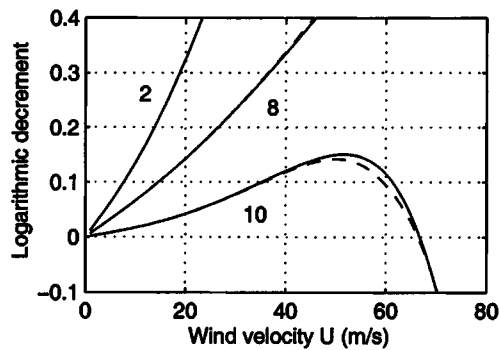
Closed-Form Solution of Two-Degree-of-Freedom Coupled Flutter

The equations of motion of a spring-supported bridge section model with heave and torsional degrees of freedom are given as

$$\mathbf{M}\ddot{\mathbf{q}} + \mathbf{C}\dot{\mathbf{q}} + \mathbf{K}\mathbf{q} = \frac{1}{2}\rho U^2 \left(\mathbf{A}_s \mathbf{q} + \frac{b}{U} \mathbf{A}_d \dot{\mathbf{q}} \right) \quad (23)$$



(a) Frequency vs. wind velocity



(b) Damping ratio vs. wind velocity

Fig. 14. Eigenvalue loci of the example suspension bridge with structural modes 2, 8, and 10 (--- and — are with and without coupled terms of structural mode 8 with other structural modes): (a) frequency versus wind velocity and (b) damping ratio versus wind velocity

where

$$\mathbf{M} = \begin{bmatrix} m_h & 0 \\ 0 & I_\alpha \end{bmatrix}; \quad \mathbf{C} = \begin{bmatrix} 2m_h \xi_h \omega_h & 0 \\ 0 & 2I_\alpha \xi_\alpha \omega_\alpha \end{bmatrix} \quad (24)$$

$$\mathbf{K} = \begin{bmatrix} m_h \omega_h^2 & 0 \\ 0 & I_\alpha \omega_\alpha^2 \end{bmatrix}; \quad \mathbf{q} = \begin{bmatrix} h \\ \alpha \end{bmatrix} \quad (25)$$

$$\mathbf{A}_s = \begin{bmatrix} 2k^2 H_4^*(k) & 2k^2 b H_3^*(k) \\ 2k^2 b A_4^*(k) & 2k^2 b^2 A_3^*(k) \end{bmatrix}$$

$$\mathbf{A}_d = \begin{bmatrix} 2k H_1^*(k) & 2kb H_2^*(k) \\ 2kb A_1^*(k) & 2kb^2 A_2^*(k) \end{bmatrix}$$

m_h and I_α = the mass and mass moment of inertia per unit length of the bridge deck, ω_h and ω_α ; ξ_h and ξ_α = mechanical circular frequencies and damping ratios in the heaving and torsional directions, respectively, H_j^* ; A_j^* ($j=1,2,3,4$) = the flutter derivatives, which can be identified through wind tunnel tests; and h and α = the heaving (downward) and torsional (nose-up) displacements.

The eigenvalues and eigenvectors of the bridge section system without the coupled self-excited forces can be expressed in an explicit form as

$$\omega_{h0}^2 = \omega_h^2 - \rho \omega_{h0}^2 b^2 H_4^*(k_{h0}) / m_h \quad (26)$$

$$\xi_{h0} = \xi_h \omega_h / \omega_{h0} - \rho b^2 H_1^*(k_{h0}) / (2m_h)$$

$$\omega_{\alpha 0}^2 = \omega_\alpha^2 - \rho \omega_{\alpha 0}^2 b^4 A_3^*(k_{\alpha 0}) / I_\alpha \quad (27)$$

$$\xi_{\alpha 0} = \xi_\alpha \omega_\alpha / \omega_{\alpha 0} - \rho b^4 A_2^*(k_{\alpha 0}) / (2I_\alpha)$$

$$\lambda_j = \lambda_{h0}, \lambda_{\alpha 0}; \quad \Phi_j = \Phi_{h0}, \Phi_{\alpha 0} \quad (28)$$

$$\lambda_{h0} = -\xi_{h0} \omega_{h0} + i \omega_{h0} \sqrt{1 - \xi_{h0}^2} \quad (29)$$

$$\lambda_{\alpha 0} = -\xi_{\alpha 0} \omega_{\alpha 0} + i \omega_{\alpha 0} \sqrt{1 - \xi_{\alpha 0}^2}$$

$$\Phi_{h0} = \begin{bmatrix} h \\ \alpha \\ \dot{h} \\ \dot{\alpha} \end{bmatrix} = \begin{bmatrix} 1 \\ 0 \\ \lambda_{h0} \\ 0 \end{bmatrix}; \quad \Phi_{\alpha 0} = \begin{bmatrix} h \\ \alpha \\ \dot{h} \\ \dot{\alpha} \end{bmatrix} = \begin{bmatrix} 0 \\ 1 \\ 0 \\ \lambda_{\alpha 0} \end{bmatrix} \quad (30)$$

The equivalent eigenvalue equation of the system without the coupled self-excited forces is given as

$$\mathbf{A}\Phi_i = \lambda_j \Phi_j \quad (31)$$

where

$$\mathbf{A} = \begin{bmatrix} 0 & 0 & 1 & 0 \\ 0 & 0 & 0 & 1 \\ -\omega_{h0}^2 & 0 & -2\xi_{h0}\omega_{h0} & 0 \\ 0 & -\omega_{\alpha0}^2 & 0 & -2\xi_{\alpha0}\omega_{\alpha0} \end{bmatrix} \quad (32)$$

The eigenvalues and eigenvectors of the system with the coupled self-excited forces can be estimated through a complex eigenvalue analysis based on Eq. (23). Here, a perturbation series solution is presented at the wind velocity range where the frequencies in heaving and torsional branches are closely aligned. The perturbation series solution renders more physical insight into the influence of coupled self-excited forces on bridge aeroelastic behavior. Choosing the system without the coupled self-excited forces as the unperturbed system, the perturbed system described in Eq. (23), involving the contribution of coupled self-excited forces, can be expressed in terms of the eigenvalue problem defined in Eq. (2) with

$$\mathbf{A} + \epsilon \mathbf{A}_0 = \begin{bmatrix} \mathbf{0} & \mathbf{I} \\ -\mathbf{M}^{-1} \left(\mathbf{K} - \frac{1}{2} \rho U^2 \mathbf{A}_s \right) & -\mathbf{M}^{-1} \left(\mathbf{C} - \frac{1}{2} \rho b \mathbf{A}_d \right) \end{bmatrix} \quad (33)$$

The frequency-dependent aerodynamic matrices \mathbf{A}_s and \mathbf{A}_d can be approximated as constant matrices defined at known re-

duced frequencies corresponding to the frequencies of the unperturbed system:

$$\mathbf{A}_s = \begin{bmatrix} 2k_{h0}^2 H_4^*(k_{h0}) & 2k_{h\alpha0}^2 b H_3^*(k_{h\alpha0}) \\ 2k_{h\alpha0}^2 b A_4^*(k_{h\alpha0}) & 2k_{\alpha0}^2 b^2 A_3^*(k_{\alpha0}) \end{bmatrix} \quad (34)$$

$$\mathbf{A}_d = \begin{bmatrix} 2k_{h0} H_1^*(k_{h0}) & 2k_{h\alpha0} b H_2^*(k_{h\alpha0}) \\ 2k_{h\alpha0} b A_1^*(k_{h\alpha0}) & 2k_{\alpha0} b^2 A_2^*(k_{\alpha0}) \end{bmatrix}$$

where

$$k_{h0} = \omega_{h0} b / U; \quad k_{\alpha0} = \omega_{\alpha0} b / U; \quad k_{h\alpha0} = \omega_{h\alpha0} b / U \quad (35)$$

$$\omega_{h\alpha0} = \frac{1}{2} (\omega_{h0} + \omega_{\alpha0})$$

This approximation in \mathbf{A}_s and \mathbf{A}_d is generally acceptable based on the fact that the coupled self-excited forces only slightly influence the frequencies, and that the aerodynamic matrices are not sensitive to the changes in the reduced frequency. This approximation is particularly valid for the region where the frequencies in heaving and torsional branches are adjacent, which is exactly the region in which the perturbation series solution is being applied.

Accordingly, the perturbation in the system matrix is approximated by

$$\epsilon \mathbf{A}_0 = \rho \omega_{h\alpha0} b^3 \begin{bmatrix} 0 & 0 & 0 & 0 \\ 0 & 0 & 0 & 0 \\ 0 & \omega_{h\alpha0} H_3^*(k_{h\alpha0}) / m_h & 0 & H_2^*(k_{h\alpha0}) / m_h \\ \omega_{h\alpha0} A_4^*(k_{h\alpha0}) / I_\alpha & 0 & A_1^*(k_{h\alpha0}) / I_\alpha & 0 \end{bmatrix} \quad (36)$$

By expressing the eigenvectors of the perturbed system in terms of those of the unperturbed system, i.e., $\Phi_j' = D_1 \Phi_1 + D_2 \Phi_2 = \Gamma \mathbf{D}$, the eigenvalue equations of the perturbed system, i.e., $\lambda_j' = \lambda_h', \lambda_\alpha'$ are given by $(\mathbf{A} + \epsilon \mathbf{H}) \mathbf{D} = \lambda_j' \mathbf{D}$ in which $\mathbf{A} = \text{diag}[\lambda_{h0}, \lambda_{\alpha0}]$, and

$$\epsilon \mathbf{H} = \Gamma_L \epsilon \mathbf{A}_0 \Gamma = \rho \omega_{h\alpha0} b^3 \begin{bmatrix} 0 & -i(\omega_{h\alpha0} H_3^* + \lambda_{\alpha0} H_2^*) / (2m_h \omega_{h0}^D) \\ -i(\omega_{h\alpha0} A_4^* + \lambda_{h0} A_1^*) / (2I_\alpha \omega_{\alpha0}^D) & 0 \end{bmatrix} \quad (37)$$

where

$$\Gamma_L = [\Phi_{h0L} \quad \Phi_{\alpha0L}]^T \quad (38)$$

$$\Phi_{h0L} = \frac{-i}{2\omega_{h0}^D} \begin{bmatrix} -\omega_{h0}^2 / \lambda_{h0} & 0 & 1 & 0 \end{bmatrix} \quad (39)$$

$$\Phi_{\alpha0L} = \frac{-i}{2\omega_{\alpha0}^D} \begin{bmatrix} 0 & -\omega_{\alpha0}^2 / \lambda_{\alpha0} & 0 & 1 \end{bmatrix}$$

$$\omega_{h0}^D = \omega_{h0} \sqrt{1 - \xi_{h0}^2}; \quad \omega_{\alpha0}^D = \omega_{\alpha0} \sqrt{1 - \xi_{\alpha0}^2} \quad (40)$$

and the superscript T denotes the matrix transpose operator.

By solving Eq. (5) with the aforementioned coefficient matrix, the eigenvalues and eigenvectors with coupled self-excited forces can be readily determined based on Eqs. (9) and (10), which are given in terms of the eigenvalues and eigenvectors without the

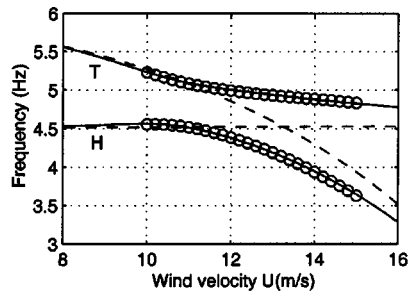
coupled self-excited forces and the coupled flutter derivatives H_2^* , H_3^* , A_1^* , and A_4^* .

At the wind velocity range where the frequencies in heaving and torsional branches of the unperturbed system are very close, we have $\omega_{h\alpha0} \approx \omega_{h0} \approx \omega_{\alpha0}$ and the matrix $\epsilon \mathbf{H}$ can be further approximated as

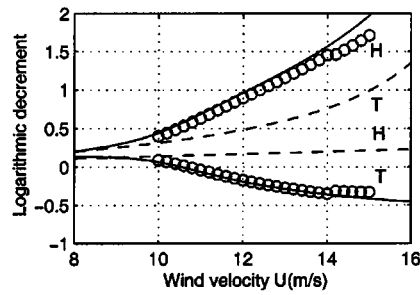
$$\epsilon \mathbf{H} \approx \rho \omega_{h\alpha0} b^3 \begin{bmatrix} 0 & (H_2^* - iH_3^*) / (2m_h) \\ (A_1^* - iA_4^*) / (2I_\alpha) & 0 \end{bmatrix} \quad (41)$$

and the veering condition of the frequency loci of the heaving and torsional branches can thus be approximately expressed in an explicit form

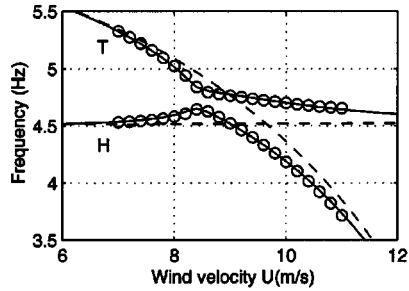
$$d = \frac{|\xi_{h0} - \xi_{\alpha0}|}{\rho b^3 / \sqrt{m_h I_\alpha} \{ [(A_1^*)^2 + (A_4^*)^2] [(H_2^*)^2 + (H_3^*)^2] \}^{1/4}} \leq O(1) \quad (42)$$



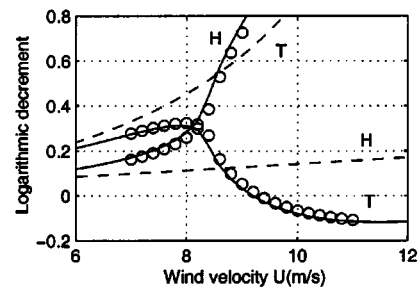
(a) Frequency vs. wind velocity (Case A)



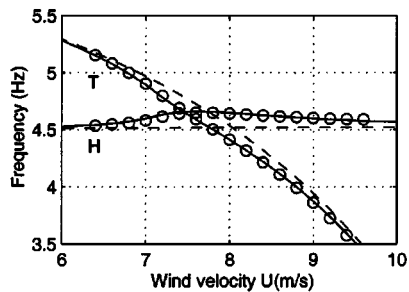
(b) Damping ratio vs. wind velocity (Case A)



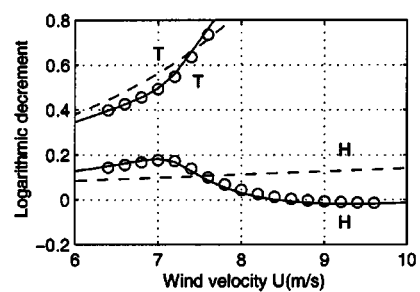
(c) Frequency vs. wind velocity (Case B)



(d) Damping ratio vs. wind velocity (Case B)



(e) Frequency vs. wind velocity (Case C)



(f) Damping ratio vs. wind velocity (Case C)

Fig. 16. Comparison of eigenvalue loci of heaving and torsional mode branches (— and — are calculated by complex eigenvalue analysis with and without coupled self-excited forces; circles are calculated by perturbation analysis): (a) frequency versus wind velocity (Case A); (b) damping ratio versus wind velocity (Case A); (c) frequency versus wind velocity (Case B); (d) damping ratio versus wind velocity (Case B); (e) frequency versus wind velocity (Case C); and (f) damping ratio versus wind velocity (Case C)

Heaving Branch Coupled Flutter

Recent studies of coupled flutter using spring-supported bridge section models have shown that the heaving branch may also be the origin of so-called heaving branch coupled flutter (Matsumoto et al. 1999). The following discussion will highlight the physics of this type of flutter from the viewpoint of curve veering of frequency loci.

A spring-supported bridge section model with heave and torsional degrees of freedom having the following parameters was used to investigate heaving branch flutter. These are: b

Table 4. Comparison of Flutter Conditions

Case no.	Branch	U_{cr} (m/s)	f (Hz)	U_{cr}/fB	$h/B\alpha$	$\phi(h) - \phi(\alpha)$ (degrees)
A	Torsion	10.57	5.14	13.71	0.68	11.05
B	Torsion	9.19	4.76	12.87	1.30	23.03
C	Heaving	8.41	4.63	12.12	2.07	41.27

$= 0.075$ m, $m_h = 2$ kg, $I_\alpha = 5. \cdot 10^{-3}$ kg \cdot m, $f_h = 4.5$ Hz, $f_\alpha = 6$ Hz, and $\xi_h = \xi_\alpha = 0.32\%$. The self-excited forces are given in three different ways for comparison purpose: case A: All flutter derivatives were calculated through the Theodorsen function, case B: All flutter derivatives were the same as case A except that A_2^* and A_3^* were twice those in case A, case C: All flutter derivatives were the same as case A except that A_2^* and A_3^* were three times those in case A. The preceding changes in A_2^* and A_3^* was to simply simulate cases of different bridge sections with distinct aerodynamic characteristics leading to different flutter behavior.

Fig. 16 shows the frequency and damping ratio loci versus the mean wind velocity for these three cases calculated through the complex eigenvalue analysis (see the Appendix). The solid and dashed lines in Fig. 16 are the results with and without the consideration of coupled self-excited forces presented by H_2^* , H_3^* , A_1^* , and A_4^* . Without the coupled self-excited forces, the two frequency loci intersect in these three cases. The coupled self-excited forces result in the separation of two frequency loci. In cases A and B, a coupled flutter is initiated from the torsional

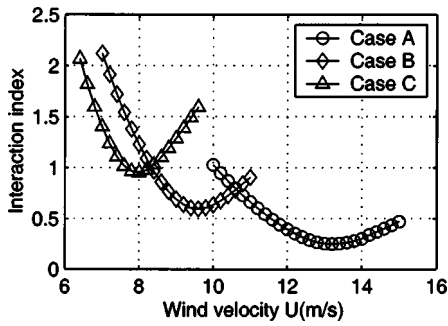


Fig. 17. Interaction index of heaving and torsional branches

mode branch. The curve veering phenomenon is noted in the frequency loci in both cases. In case C, the coupled self-excited forces only slightly change the eigenvalues of this system, and the frequency loci remain intersected. As a consequence, a coupled flutter is initiated from the heaving mode branch in case C. Table 4 compares the coupled flutter conditions including the flutter mode branch, critical flutter velocity, frequency, reduced velocity, amplitude ratio, and phase difference between heaving and torsional motions in the coupled flutter mode for each case. It is noted that the coupled flutter motion in these three cases is similar, i.e., the torsional motion lags the coupled heaving motion.

The eigenvalue loci calculated by the perturbation analysis are also presented in Fig. 16 as indicated by circles. Results illustrated the accuracy of the approximation of the self-excited forces and the perturbation solution in a closed form. Fig. 17 shows the mode interaction index [Eq. (15)] for these three cases indicating the influence of the coupled self-excited forces at the wind velocity region where two frequency loci are close each other. As alluded to earlier, a lower value corresponds to a stronger interaction. The mode interaction decreases successively in cases A, B, and C. In both cases A and B, a strong interaction between the heaving and torsional motions results in curve veering. The result of case C indicates that a heaving branch flutter corresponds to the intersection of frequency loci. Comparing these three cases in light of the eigenvalue loci, coupled motions in terms of the amplitude ratio and phase difference corresponding to the branch where the coupled flutter is initiated, flutter condition at the critical flutter velocity, and the role of the self-excited forces to the development of aerodynamic damping, it is concluded that the heaving branch coupled flutter is physically consistent with the generally observed torsional branch coupled flutter. Similar to the torsional branch coupled flutter, the heaving branch coupled flutter, resulting from the negative aerodynamic damping introduced by the coupled self-excited forces, shows coupled heaving and torsional motions in which the torsional motion lags the heaving motion.

Concluding Remarks

The curve veering phenomenon of frequency loci of bridges with aeroelastic effects was studied utilizing cable-stayed and suspension bridges. A perturbation series solution that includes the adjacent complex eigenvectors in the zeroth-order expansion was presented, and its effectiveness and accuracy in estimating the variations of the complex eigenvalues of dynamic systems, due to small changes in the system parameters, was demonstrated. The condition for veering of frequency loci was quantified by modal interaction parameter, and its efficacy was illustrated by the way

of examples. In order to better understand the curve veering of frequency loci, a 2DOF structure-TMD system was first studied. The perturbation in system parameters was chosen as the coupled terms between the structure and the TMD. It was demonstrated that the frequency loci may veer or intersect depending on the damping ratio of the TMD, which controlled the interaction level between the TMD and the structure. For long-span bridges, the perturbation in system parameters was chosen as the aerodynamic coupling terms between the structural modes. It was found that the curve veering of adjacent bridge frequency loci was due to the influence of strong aerodynamic coupling. The detailed discussion on the curve veering of frequency loci offered new insights into the dynamics of a structure-TMD system, provided a correct explanation of the results of the multimode coupled flutter analyses of long span bridges, and helped in improved understanding of the underlying physics of their aeroelastic behavior.

Heaving branch coupled flutter observed in spring-supported bridge section models was investigated from the viewpoint of curve veering. Closed-form expressions were developed to describe the eigenvalues of the coupled system and a veering condition of frequency loci. It was revealed that the heaving mode branch flutter corresponded to the intersection of frequency loci of heaving and torsional mode branches due to the weak influence of the coupled self-excited forces. It was noted that the heaving mode branch flutter was physically consistent with the generally observed torsional mode branch flutter.

Acknowledgments

The support for this work was provided in part by NSF Grant Nos. CMS 9402196 and CMS 95-03779. This support is gratefully acknowledged. The writers are thankful to Tracy Kijewski for her comments on the manuscript.

Appendix: Eigenvalue Analysis of Bridges with Aeroelastic Effects

For the sake of completeness and clarity, the framework for estimating the eigenvalues of bridges with aeroelastic effects is briefly outlined here. The approach employs time-invariant state-space formulations with augmented aerodynamic states. A more detailed discussion can be found in literature (e.g., Chen et al. 2000; Chen et al. 2001).

The governing equations of a bridge motion in modal coordinates are given by

$$\mathbf{M}\ddot{\mathbf{q}} + \mathbf{C}\dot{\mathbf{q}} + \mathbf{K}\mathbf{q} = \mathbf{Q}_{se} + \mathbf{Q}_b \quad (43)$$

where \mathbf{M} , \mathbf{C} , and \mathbf{K} = the generalized mass, damping, and stiffness matrices, respectively; \mathbf{q} , \mathbf{Q}_{se} , and \mathbf{Q}_b = the modal coordinates, the generalized self-excited, and buffeting force vectors, respectively; and the over-dot denotes partial differentiation with respect to time. The buffeting term has been excluded in the following discussion since it does not influence the bridge modal properties in the linear aerodynamic analysis.

The self-excited forces corresponding to the steady-state sinusoidal motion $\mathbf{q}(t) = \bar{\mathbf{q}}e^{i\omega t}$ can be approximated in terms of a rational function as

$$\begin{aligned} \mathbf{Q}_{se}(t) &= \frac{1}{2} \rho U^2 (\mathbf{A}_s + (ik)\mathbf{A}_d) \bar{\mathbf{q}} e^{i\omega t} \\ &= \frac{1}{2} \rho U^2 \left(\mathbf{A}_1 + (ik)\mathbf{A}_2 + (ik)^2\mathbf{A}_3 + \sum_{\ell=1}^m \frac{(ik)\mathbf{A}_{\ell+3}}{ik + d_\ell} \right) \bar{\mathbf{q}} e^{i\omega t} \end{aligned} \quad (44)$$

where ρ = the air density, U = the mean wind velocity, $k = \omega b/U$ = the reduced frequency, $B = 2b$ = the bridge deck width, ω = the circular frequency of motion, i = the imaginary unit $\sqrt{-1}$, $\mathbf{A}_1, \mathbf{A}_2, \mathbf{A}_3, \mathbf{A}_{\ell+3}$ and d_ℓ ($d_\ell \geq 0; \ell = 1, 2, \dots, m$) = frequency-independent matrices and parameters, and m = the order of the rational terms. This approximation can be determined by curve-fitting experimental data of the aerodynamic matrices $\mathbf{A}_s(ik)$ and $\mathbf{A}_d(ik)$ defined at a set of discretized reduced frequencies k_j ($j = 1, 2, \dots$) using a least-square approach. $\mathbf{A}_s(ik)$ and $\mathbf{A}_d(ik)$ are functions of the mode shapes and the flutter derivatives (e.g., Chen et al. 2001).

After some manipulations, the equations of motions at the mean wind velocity U are expressed in terms of the following frequency-independent, time-invariant state-space equations:

$$\dot{\mathbf{Y}}(t) = \mathbf{A}\mathbf{Y}(t) \quad (45)$$

where

$$\mathbf{A} = \begin{bmatrix} \mathbf{0} & \mathbf{I} & \mathbf{0} & \cdots & \mathbf{0} \\ -\bar{\mathbf{M}}^{-1}\bar{\mathbf{K}} & -\bar{\mathbf{M}}^{-1}\bar{\mathbf{C}} & \frac{1}{2}\rho U^2\bar{\mathbf{M}}^{-1} & \cdots & \frac{1}{2}\rho U^2\bar{\mathbf{M}}^{-1} \\ \mathbf{0} & \mathbf{A}_4 & -\frac{U}{b}d_1\mathbf{I} & \cdots & \mathbf{0} \\ \vdots & \vdots & \vdots & & \vdots \\ \mathbf{0} & \mathbf{A}_{3+m} & \mathbf{0} & \cdots & -\frac{U}{b}d_m\mathbf{I} \end{bmatrix}$$

$$\mathbf{Y} = \begin{bmatrix} \mathbf{q} \\ \dot{\mathbf{q}} \\ \mathbf{q}_{sel} \\ \vdots \\ \mathbf{q}_{sem} \end{bmatrix} \quad (46)$$

$$\bar{\mathbf{M}} = \mathbf{M} - \frac{1}{2}\rho b^2\mathbf{A}_3; \quad \bar{\mathbf{C}} = \mathbf{C} - \frac{1}{2}\rho U b\mathbf{A}_2; \quad \bar{\mathbf{K}} = \mathbf{K} - \frac{1}{2}\rho U^2\mathbf{A}_1 \quad (47)$$

\mathbf{q}_{sel} ($\ell = 1, 2, \dots, m$) are the augmented unsteady aerodynamic states.

The eigenvalue problem is then expressed as

$$\mathbf{A}\Phi_j = \lambda_j\Phi_j \quad (48)$$

where λ_j and Φ_j = eigenvalue and eigenmode associated with the j th complex mode branch. The eigenvalues corresponding to structural modes can be expressed as

$$\lambda_j = -\xi_j\omega_j + i\omega_j\sqrt{1-\xi_j^2} \quad (j = 1, 2, \dots, N) \quad (49)$$

where ω_j and ξ_j = frequency and damping ratio in the j th complex mode branch, which include aeroelastic effects.

References

- Anderson, P. W. (1958). "Absence of diffusion in certain random lattices." *Phys. Rev.*, 109, 1492–1505.
- Chen, P.-T., and Ginsberg, J. H. (1992). "On the relationship between veering of eigenvalue loci and parameter sensitivity of eigenfunctions." *J. Vibr. Acoust.*, 114, 141–148.
- Chen, X., Kareem, A., and Matsumoto, M. (2001). "Multimode coupled flutter and buffeting analysis of long-span bridges." *J. Wind. Eng. Ind. Aerodyn.*, 89(7–8), 649–664.
- Chen, X., Matsumoto, M., and Kareem, A. (2000). "Aerodynamic coupling effects on the flutter and buffeting of bridges." *J. Eng. Mech.*, 126(1), 17–26.
- Katsuchi, H., Jones, N. P., and Scanlan, R. H. (1999). "Multimode coupled flutter and buffeting analysis of the Akashi-Kaikyo Bridge." *J. Struct. Eng.*, 125(1), 60–70.
- Leissa, A. W. (1974). "On a curve veering aberration." *J. Appl. Math. Phys. (ZAMP)*, 25, 99–112.
- Matsumoto, M., Yoshizumi, F., Yabutani, T., Abe, K., and Nakajima, N. (1999). "Flutter stabilization and heaving-branch flutter." *J. Wind. Eng. Ind. Aerodyn.*, 83, 283–299.
- Miyata, T., and Yamada, H. (1988). "Coupled flutter estimate of a suspension bridge." *Proc., Int. Colloquium on Bluff Body Aerodyn. and its Appl.*, Japan Association for Wind Engineering, Tokyo, 485–492.
- Morard, H. J.-P., and Ohayon, R. (1995). *Fluid structure interaction*, Wiley, New York.
- Nair, P. S., and Durvasula, S. (1973). "On quasi-degeneracies in plate vibration problems." *Int. J. Mech. Sci.*, 15, 975–986.
- Perkins, N. C., and Mote, Jr., C. D. (1986). "Comments on curve veering in eigenvalue problems." *J. Sound Vib.*, 106, 451–463.
- Pierre, C. (1988). "Mode localization and eigenvalue loci veering phenomena in disordered structures." *J. Sound Vib.*, 126, 485–502.